sciendo

Int. J. of Applied Mechanics and Engineering, 2020, vol.25, No.1, pp.52-74
DOI: 10.2478/ijame-2020-0005

THE CHARACTERISTICS OF SELECTED TRIAXIALITY MEASURES OF THE STRESSES FOR A C(T) SPECIMEN DOMINATED BY THE PLANE STRAIN STATE

M. GRABA
Kielce University and Technology
Faculty of Mechatronics and Mechanical Engineering
Department of Manufacturing Engineering and Metrology
Al. 1000-lecia PP 7, 25-314 Kielce, POLAND
E-mail: mgraba@tu.kielce.pl

The paper presents a comprehensive analysis of the stress field and selected triaxiality parameters near the crack tip for C(T) specimen dominated by the plane strain state using the finite element method. It includes some theoretical information about elastic-plastic fracture mechanics, the basics of the FEM modeling and presentation of the numerical results. The FEM analysis includes calculations with large strain assumptions. The influence of the external load and crack length is discussed. Additional elements of the paper are a qualitative assessment of the size of plastic zones and the crack tip opening displacement.

Key words: fracture mechanics, C(T), FEM, stress triaxiality parameter, Lode parameters, constraints, plane strain.

1. Introduction

The analysis of the fracture process of elastic-plastic materials was for a long period of time based on experimental research and purely theoretical considerations. Different researchers used different types of specimens, looking for appropriate possibilities to assess the fracture process. The sphere of experimental research was finally ordered, and for proper research, a number of normative documents were prepared, which regulate what the type of specimen, which should be used, what dimensions it should have. Examples include the ASTM standards [1,2], BS standards [3,4], and even the Polish Standard [5], in force for many years, which allows testing with less restrictions than the ASTM standards [1,2], especially that the ASTM standards regulate in detail the number of valid points. The basic types of specimens that find application in fracture mechanics to determine fracture toughness are a three-point bending specimen denoted by SEN(B) and a compact specimen, denoted by C(T).

The SEN(B) specimen geometry is more often used in the research, which can often be conditioned by the tooling of the testing machine, however the C(T) specimen has also found application in many aspects of fracture. For example, in [6-8], various researchers used the C(T) specimen to assess the cracking phenomena and fracture toughness of various materials. In scientific papers [9-11], the development of research methods, as well as the need for calibration used in experimental designs, were discussed by authors to define the method of determining critical fracture toughness values based on C(T) specimens. In [12] presented in 2012, Zhu and Joyce discussed an overview of methods for determining fracture toughness using the C(T) and SEN(B) specimens, alongside the C(T) geometry, indicating the need to consider the influence of geometric constraints in formulas approximating the equations of the *J-R* curves. The parameters of geometrical constraints mentioned in the paper [12] include the *Q*-stress (described as *Q*-parameter, which was defined by O'Dowd and Shih [13-14]) and the A_2 parameter [15] (described also as A_2 amplitude discussed by Yang *et al*.). It should be remembered, however, that both parameters – Q and A_2 are determined by numerical calculations with the assumption of small deformations and displacements, as well as both parameters are a correction of the HRR solution presented in 1968 [16, 17] and improve the description of stress fields near the crack tip taking into account the influence of the other parts of the asymptotic solution.

2. Stress fields near the crack tip

A characteristic feature of the HRR solution is the singularity of stresses (Fig.1a). Stresses as they approach the tip of the crack tend to infinity. However, in the real structural element, the stresses in front of the crack tip are finite – such a distribution in numerical calculations is obtained by assuming large strains and large displacements (Fig.1a and Fig.1b), which in the case of stress distribution leads to reach a maximum of the crack opening stress at a specific distance from the crack tip [18, 19] (Fig.1a and Fig.1b), as mentioned in two subsequent papers [20,21]. "The value of this maximum as well as its position near the crack tip was used in [18] in the proposal of a modified crack criterion based on the RKR hypothesis [19]. The mentioned fracture criterion also uses the Q-stresses defined by O'Dowd and Shih [13, 14]. It should be noted that the level of maximum stresses and their position near the crack tip depends on the material characteristics, geometry, and external load which is also shown in [18]." [20,21].

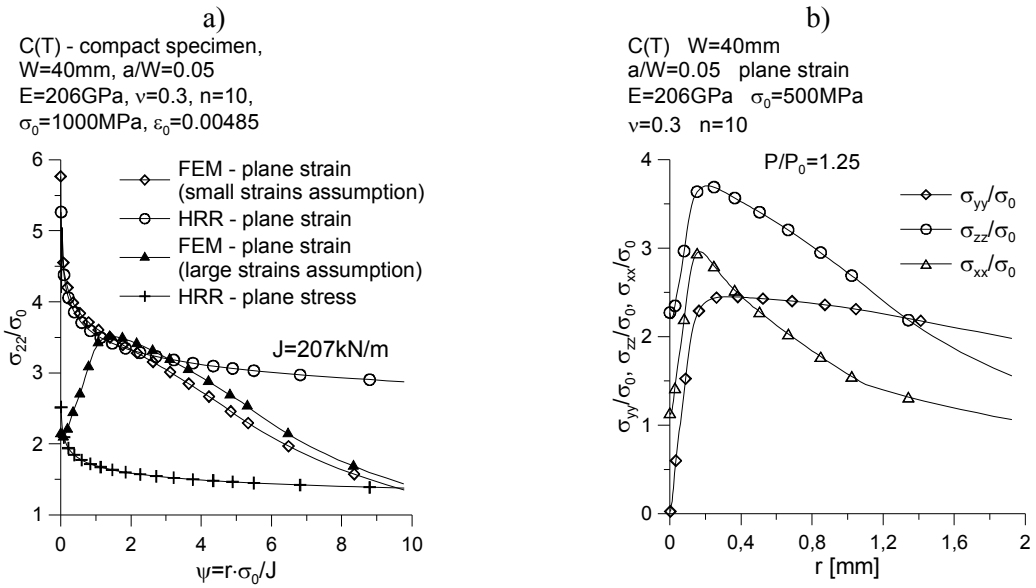

Fig.1. a) The stress distribution near the crack tip for C(T) specimen – comparison the crack opening stress for the HRR solution (plane stress and plane strain condition) with numerical results for plane strain condition with assumption the small and large strains [20,21]; b) Distribution of the normal stress tensor components near the crack tip for C(T) specimen.

2.1. Basic parameters of in-plane geometric constraints

The results of the numerical calculations arising from the relevant assumptions, leading to the determination of:

- *Q*- stresses – it is the difference between the numerically estimated stresses and the stresses determined by the HRR solution, normalized by the yield point – $Q=(\sigma_{22\_FEM}-\sigma_{22\_HRR})/\sigma_0$ – determined for $\varphi=0$ direction for normalized distance from the crack tip $x=2\cdot J/\sigma_0$[13, 14] (small strain assumptions);
- maximum crack tip opening $\xi_o=\sigma_{22_max}/\sigma_0$and their normalized position relative to the crack tip, denoted by $\psi_o=x_{22\_max}\cdot\sigma_0/J$ [18, 19] (large strain assumptions),

allow to develop a full catalogue of numerical solutions that will make it possible to estimate these parameters without having to perform numerical calculations. In the case of a compact specimen, such a catalog was shown by [20,21].

As indicated by the numerical calculations and conclusions given in [20,21], *Q* stresses depend on the level of external load, the geometry of the structural element (relative crack length *a/W*) and material characteristics (expressed by the work hardening exponent *n* and the yield stress σ_0). In the case of maximum

stresses opening the crack surfaces and their relative position with respect to the crack tip, the effect of the external load is not as significant as the effect of the relative crack length, however these parameters are significantly sensitive to the change in material properties. Figures 2 and 3 present the selected results of the numerical calculations for C(T) type specimens (elaborated and discussed in [20, 21]), presenting the effect of external load, material characteristics and relative crack length on the selected parameters of geometric constraints mentioned above, which were determined numerically with the assumption of small and large deformations in the FEM analysis, respectively. The assessment of the impact of variables (such as geometry, material characteristics or external load) on the level of selected parameters of the in-plane constraints is left to the reader and referred to [21], from which the drawings were taken, where the reader also finds simple approximation formulas for estimating the value of selected in-plane constraint parameters, without the need for tedious FEM calculations.

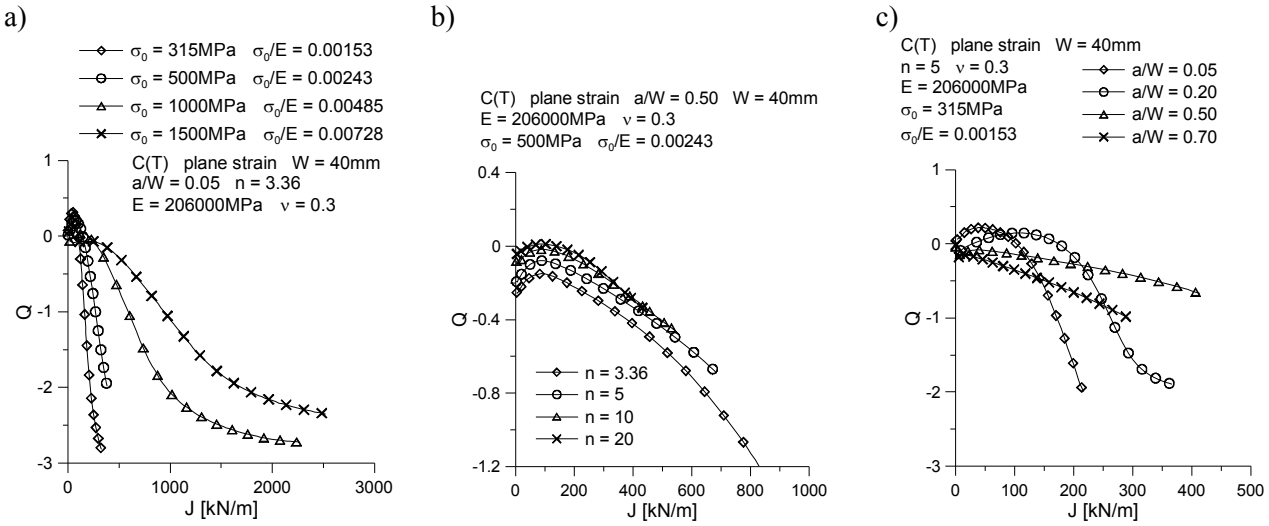

Fig.2.The influence of the yield stress σ_0 (a), strain hardening exponent n (b) and relative crack length a/W(c) on the J-Q trajectories for compact specimens – results for the whole spectrum of the external load – based on [20, 21].

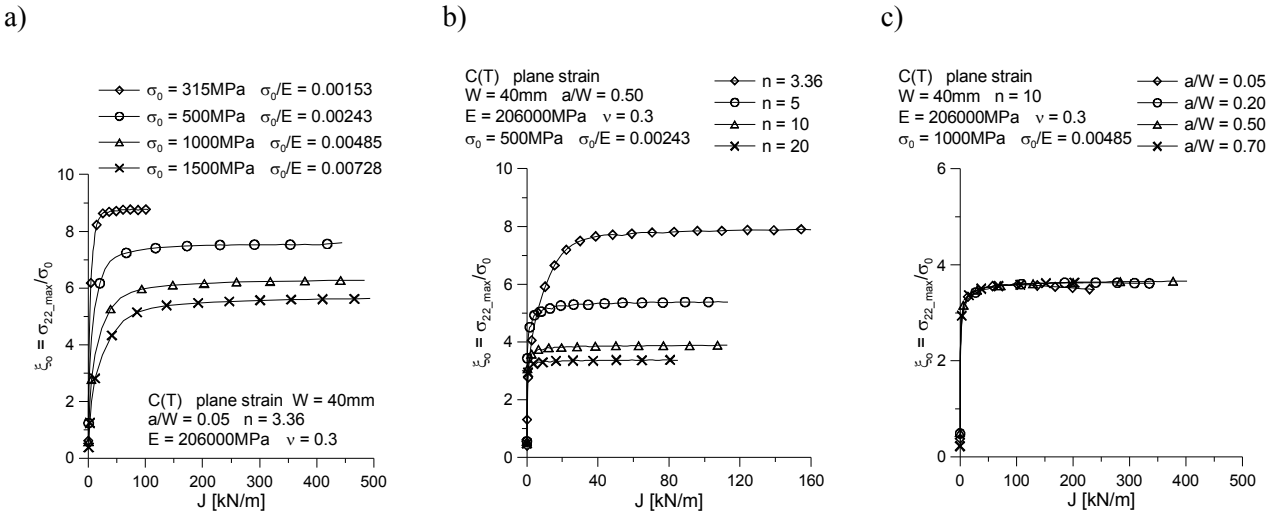

Fig.3. The influence of the yield stress σ_0 (a), strain hardening exponent n (b) and relative crack length a/W (c) on the maximum crack opening stress ($\xi_o=\sigma_{22\_max}/\sigma_0$) for compact specimens – results for the whole spectrum of external load – based on [20, 21].

Similar sets of in-plane constraints measurements for many other basic geometries used in the studies of fracture mechanics can be found in [22-26]. In addition to theoretical considerations, assessing the impact of external load, geometry or material characteristics, the simplified approximation formulas were also given in these papers, so that the estimation of the measurement of in-plane constraints was possible without the need to perform the FEM calculations.

2.2. Selected stress triaxiality parameters

The considerations regarding the characteristics of the state of stress near the crack tip, requires the isotropic material model, which allows to formulate the in terms of three invariants of the stress tensor $[\sigma]$, defined by following equations [27], respectively

$$p = -\sigma_m = -\frac{1}{3} tr\left([\sigma]\right) = -\frac{1}{3}\left(\sigma_1 + \sigma_2 + \sigma_3\right), \tag{2.1}$$

$$q = \bar{\sigma} = \sigma_{eff} = \sqrt{\frac{3}{2}[S]:[S]} = \sqrt{\frac{1}{2}\left[\left(\sigma_1 - \sigma_2\right)^2 + \left(\sigma_2 - \sigma_3\right)^2 + \left(\sigma_3 - \sigma_1\right)^2\right]}, \tag{2.2}$$

$$r = \left(\frac{9}{2}[S]\cdot[S]:[S]\right)^{\frac{1}{3}} = \left[\frac{27}{2}\det\left([S]\right)\right]^{\frac{1}{3}} = \left[\frac{27}{2}\left(\sigma_1 - \sigma_m\right)\left(\sigma_2 - \sigma_m\right)\left(\sigma_3 - \sigma_m\right)\right]^{\frac{1}{3}}, \tag{2.3}$$

wherein the $[S]$ denotes the deviatoric stress tensor according to Eq.(2.4)

$$[S] = [\sigma] + p[I] \tag{2.4}$$

where the $[I]$ is the identity tensor; σ_1, σ_2, σ_3 are the principal stresses, fulfilling the following condition: $\sigma_1 \geq \sigma_2 \geq \sigma_3$. The σ_m and σ_{eff} denote the mean stress and effective stress respectively, and by r we understand the third invariant of the stress deviator. In some scientific papers, like this article, the principal stress is marked by a slightly different notation, replacing the index written with Arabic notation ("1", "2" and "3") for indexes written with Roman notation ("I", "II" and " III ").

Based on the given considerations, we can define the stress triaxiality parameter, which is generally given in the form of dimensionless hydrostatic stress denoted by η

$$\eta = \frac{-p}{q} = \frac{\sigma_m}{\bar{\sigma}}. \tag{2.5}$$

It is a quotient of mean stresses and effective stresses, quite often used in the literature for discussion about ductile fracture [28, 29]. In some papers, this quantity is indicated by a quotation in the form of a quotient σ_m/σ_{eff}. This parameter is also often used in the discussion of the triaxiality of stresses, just like the Lode angle denoted as θ, which can be related to the normalized third stress invariant denoted as ξ by following equation

$$\xi = \left(\frac{r}{q}\right)^3 = \cos\left(3\theta\right), \tag{2.6}$$

wherein the Lode angel range is $0 \leq \theta \leq \pi/3$ and the range of the normalized third stress invariant is $-1 \leq \xi \leq 1$. In some papers [27], the normalized Lode angel denoted as $\bar{\theta}$ is used in the following form

$$\bar{\theta} = 1 - \frac{60}{\pi} = 1 - \frac{2}{\pi}\arccos\left(\xi\right). \tag{2.7}$$

The values of the normalized Lode angle $\bar{\theta}$ should be included in the range $-1 \le \bar{\theta} \le 1$ [27].

Bai and Wierzbicki [30] also used another definition of the Lode parameter, denoted as L, which may be presented in the following form

$$\mathrm{L} = \mathrm{LODE} = \frac{2\sigma_2 - \sigma_1 - \sigma_3}{\sigma_1 - \sigma_3} \tag{2.8}$$

where the σ_1 and σ_3 are the maximum and the minimum principal stresses respectively. In this paper, the Lode parameter L will be referred to as an expression LODE. The Lode parameter may be related to the normalized third stress invariant ξ through the following relationship [27]

$$\xi = \mathrm{L}\frac{9 - L^2}{\sqrt{\left(L^2 + 3\right)^3}}. \tag{2.9}$$

The parameters mentioned above can be successfully used to describe the level of triaxiality of stress near the crack tip [31], or calibration the constitutive equations, which was presented by Bao and Wierzbicki or Bai and Wierzbicki [30, 32, 33], where the yield stress denoted as σ_{yld} were defined according to the next formula

$$\sigma_{yld} = \bar{\sigma}\left(\overline{\varepsilon_p}\right)\left[1 - c_\eta\left(\eta - \eta_0\right)\right]\left[c_\theta^s + \left(c_\theta^{ax} - c_\theta^s\right)\left(\gamma - \frac{\gamma^{m+1}}{m+1}\right)\right] \tag{2.10}$$

where the function $\bar{\sigma}\left(\overline{\varepsilon_p}\right)$ describes the relation between effective real stress and accumulated plastic strain; $\eta_0$denotes the reference value of the triaxiality coefficient η (see Eq.(2.5) – it can be noted, that for the case of the uniaxial tensile test, value of the η_0 is equal to *1/3* for cylindrical specimen); the parameters c_η, c_θ^s, c_θ^{ax} and *m* must be determined for specific material experimentally; the function γ may be calculated by the Bai and Wierzbicki [30,32,33] formula (this function satisfies the inequality $0 \le \gamma \le 1$, and $\gamma = 0$ for plane strain or pure shear states, or $\gamma = 1$ for axial symmetry)

$$\gamma = 6.464\left[\sec\left(\theta - \frac{\pi}{6}\right) - 1\right]. \tag{2.11}$$

The possibility of applying the above-mentioned triaxiality parameters (for which some researchers also recognize the LODE parameter and Lode angle θ, or normalized Lode angle $\bar{\theta}$) makes it necessary to develop a method for their numerical estimation (especially the development of post-processing methods for numerical results) and to discuss the changes of these parameters around the crack tip.

Therefore, the present paper focuses on the analysis of the stress level near the crack tip, the assessment of selected parameters commonly recognized as measures of stress triaxiality, as well as the assessment of the level of accumulated plastic strain. Numerical calculations were carried out for the case of plane strain state dominance (similarly to the analysis carried out in the paper by Bai *et al*. [27]), with the assumption of large deformations and a randomly chosen material model.

3. Basics of Finite Element Method (FEM) modeling

In the calculations, the C(T) specimen was modeled in accordance with the ASTM standards [1, 2] and EPRI procedures [34]. The width of the specimen was set to *W=40mm*, while the relative crack length *a/W* was taken from the set $a/W = \{0.05, 0.20, 0.70\}$, where *a* means crack length. In the calculations, the real stress-strain curve described by the power law Eq.(3.1) was used

$$\frac{\varepsilon}{\varepsilon_0} = \begin{cases} \sigma/\sigma_0 & \text{for} \quad \sigma \le \sigma_0 \\ \alpha \cdot \left(\sigma/\sigma_0\right)^n & \text{for} \quad \sigma > \sigma_0 \end{cases} \tag{3.1}$$

wherein, that the power constant $\alpha=1$, Young modulus E=206GPa, Poisson's ratio $\nu=0.3$, yield stress $\sigma_0=500$MPa, the strain hardening exponent $n=10$ [20,21]. The isotropic with J_2 plasticity theory model of the material was used for carrying out the numerical calculations.

In the Finite Element Method (FEM) analysis, using the existing axis of symmetry only half of the compact specimen was modeled (Fig.4a) [35,36] – hatched part of specimen. In order to model the actual load method, the contact issue was solved – the load of C(T) specimens was carried out with the help of a spindle (i.e. pin) (Fig.4a), characterized by diameter $\phi 10mm$, which was modeled in the form of half of the arch. An external load was applied to the pin in the form of a linearly increasing displacement [20,21].

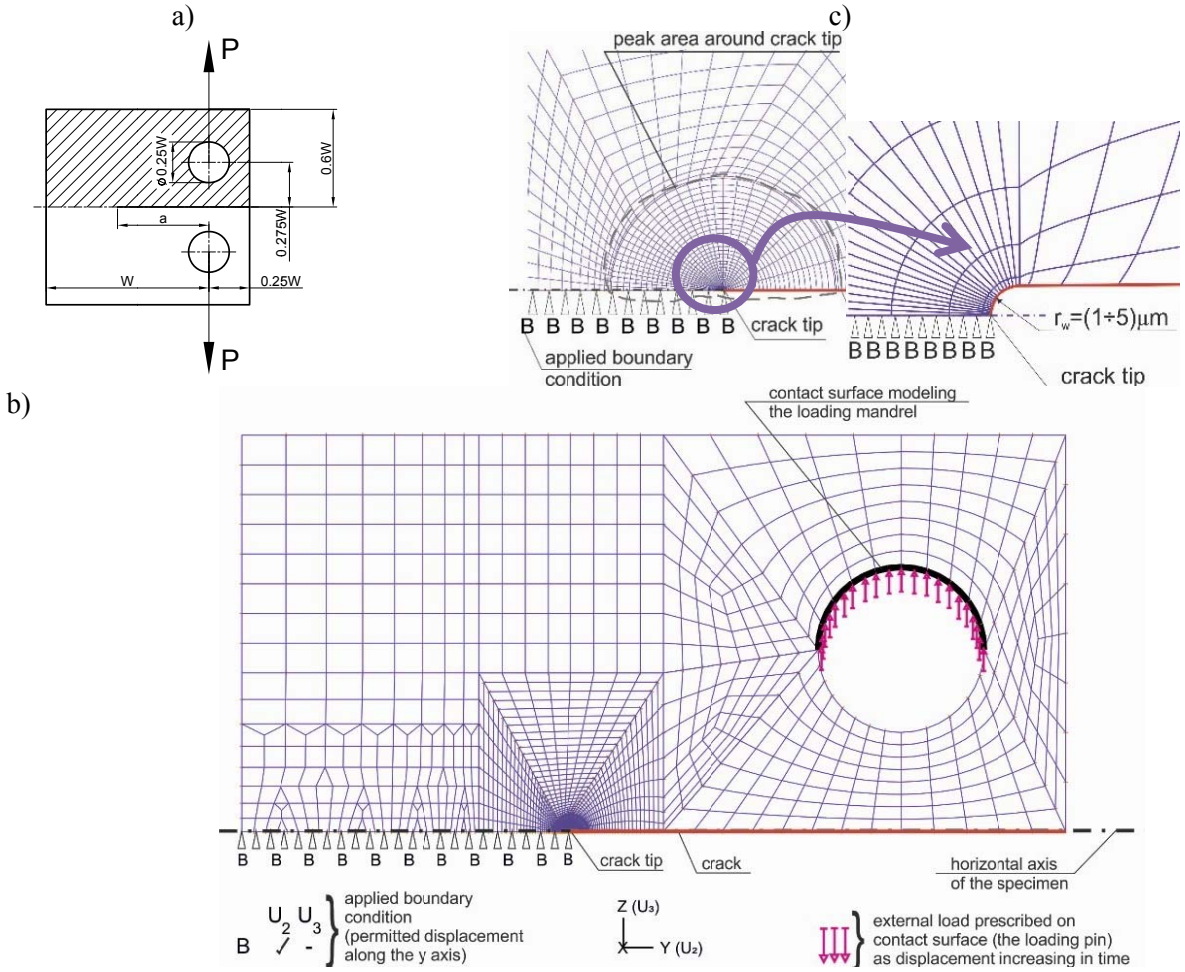

Fig.4. The C(T) specimen used in the numerical program: a) schematic technical drawing of the C(T) specimen with hatched part which were used in the FEM analysis – based on [20,21]; b) a half of the C(T) specimen with applied boundary conditions and external load; c) zoom of the peak area near crack tip and the shape of the crack tip.

The whole numerical (finite element) model of the C(T) specimen is shown on Fig.4b. The crack tip for C(T) specimen was modeled in the form of a quarter of the arch, with radius r_w equal to $5\mu m$ (the radius of the crack tip was 8000 times smaller than the width of the specimen $W=40mm$). This crack tip was divided

into 20 parts together with the density of the elements towards the edge lying in the axis of the specimen. The edge finite elements were (5÷20) times smaller than the largest elements located in the central part of the arch – see Fig.4c. For each specimen, the peak area with a radius equal to approximately (*1.0÷2.5*)*mm*, was divided into (35÷50) finite elements (FEs), wherein the smallest FE located at the crack tip was 100 times smaller than the previous one (Fig.3b). This meant that, in extreme cases, the smallest FE, located just next to the crack tip, represented about *1/70700* or *1/101000* of the width *W* of the specimen, and the largest modeling the peak area has the size about *1/707* or *1/1010* of the specimen width [20,21].

The FEM analysis was carried out with the assumption of large strains and large displacements, which is necessary to determine the maximum stresses opening the fracture surfaces – it guarantees the finite distribution of stresses near the crack tip. The FEM model was filled with nine-node Finite Elements (FEs), using the "2-D SOLID plane strain" type and "mixed" interpolation with nine Numerical Integration Points (NIP) [20, 21].

The *J*-integral, referred to as the crack driving force, or the amplitude of the singular stress field near the crack tip, was determined using the method of virtual crack length growth [20,21]. Several integrating contours were defined, taking into account the principle proposed by Guo [37] for three-dimensional solutions, where the integration contour required for the numerical estimation of the *J*-integral should be defined as “far-field contour” [37]. This approach also guarantees the invariance of the *J*-integral when assuming the analysis of large deformations and displacements. The *J*-integral values obtained using virtual crack length growth were the same as results for calculations done using the*J*-integral definition given by Rice [38], which was presented in [39], [20,21].

For the purpose of this article, in order to determine the level of limit loads, the formula (3.2), presented in [20,21] was used, based on numerical calculations previously performed. This formula allows to estimate the limit load value P_0 taking into account the plasticity limit (yield stress) σ_0 inserted in [MPa] and the relative crack length a/W [21]

$$P_0 = A_1 + A_2 \cdot \sigma_0 + A_3 \cdot \left(\frac{a}{W}\right) + A_2 \cdot \left(\sigma_0\right)^2 + A_5 \cdot \left(\frac{a}{W}\right)^2 + A_6 \cdot \sigma_0 \cdot \left(\frac{a}{W}\right) \tag{3.2}$$

where the limit load value P_0 is obtained in [kN], with the matching factor $R^2=0.993$, using the following values of approximation factors: $A_1=-933.154$, $A_2=10.262$, $A_3=9612.613$, $A_4=-5.91\cdot10^{-5}$, $A_5=-12986.874$, $A_6=-11.429$ [21]. This approach was chosen due to too large differences between the known analytical solutions [34] and the results of numerical calculations [21].

The next paragraph presents the results of numerical calculations that characterize the stress field near the crack tip in C(T) specimens (compact specimens). The reference to the relative values of the force acting on the specimen given in the chapters will refer to the cases of normalization by the value of the limit load determined for the purpose of this paper.

4. FEM results – presentation and short analysis

The obtained numerical results were first compiled in a graphical form, composing diagrams of changes in the distribution of the normal components of the stress tensor for each analyzed geometry at different levels of external load, normalized by the limit load P_0estimated according to the formula (3.2). Next, the level of effective stress σ_{eff}/σ_0, mean $\sigma_m/\sigma_0$was evaluated, and level of selected stress triaxiality parameters. Among these parameters, the quotients σ_{eff}/σ_0 and σ_m/σ_0 mentioned in the previous sentence can be distinguished, as well as the quotient of mean and effective stresses σ_m/σ_{eff}. Some researchers believe that the normalized angle Lode $\bar{\theta}$ and the Lode parameter, determined in accordance with formulas (2.7) and (2.8), denoted in this paper by LODE, are also a measure of the stress triaxiality, therefore in the second part of this paragraph these parameters were also evaluated.

4.1. Analysis of the stress field near crack tip

Conducting numerical calculations using the assumption of large strains and displacements leads to a finite stress distribution through the tip of the crack (Figs 5 and 6). As it approaches the crack tip, normal stresses

increase, reaching a maximum in a specified place. It should be noted that the highest maximum value is achieved by normal stresses opening the surface of the crack (denoted by σ_{zz}), and the lowest stress σ_{yy} coinciding with the direction of the crack – the value of this maximum is less than the maximum value of σ_{zz} stresses by about *150*%.

The maximum of the σ_{xx} stresses, acting in the direction of thickness, takes the intermediate value between the maximum σ_{zz} and σ_{yy}, generally smaller than the maximum σ_{zz} by about *75*%. The physical position of this maximum varies with the increasing external load – the higher the level of external load, the farthest from the crack tip is the maximum stress (Fig.5). It should be noted that the maximum for consecutive normal stresses denoted as σ_{zz}, σ_{yy} and σ_{xx} does not occur in the same physical distance (compare Fig.5). Farthest from the crack tip is the maximum of the crack opening stress.

In Fig.5, next to the distribution of the normal components of the stress tensor, it is also shown how the level of average stresses (denoted by σ_m) and the effective stresses σ_{eff} are changed. The mean stress σ_m, like the normal components, along with approaching the crack tip also reach the maximum (this is nothing extraordinary, it results directly from the nature of the distribution of normal components) – the physical location of this maximum in relation to the crack tip increases with the increase of the external load.
The effective stresses, however, reach the highest value near the crack tip, then along with the distance from it, their value decreases to the value equal to the yield point and remains at such a level in the entire range covered by the plastic zone, which is the result of action of the external load. It can therefore be said that the place where for the direction $\varphi=0$ the value of the effective stresses σ_{eff} is falling below the value of the yield point is the end point of the plastic zone in the mentioned direction. At the external load level $P/P_0=0.75$, the length of the plastic zone for the direction $\varphi=0$ is approximately $1 \div 2$% of the specimen width (Fig.5). The increase of the external load to the level $P/P_0=1.25$ means the increase of the plastic zone length for the direction $\varphi=0$ to at least *5*% of the width of the specimen denoted as *W*.

Figure 6 presents the changes in stress tensor components, average stresses and effective stresses listed in Fig.5, plotted against the normalized distance from the crack tip denoted by ψ. As it can be seen, in the considered range of external loads ($P/P0 = \{0.75, 1.00, 1.25\}$), the level of maximum stress opening the surfaces of the crack and other normal stress tensor components do not change with the increasing external load. The maximum value of the stress opening the fracture surfaces for the C(T) specimen with the relative crack length $a/W=0.05$ is approximately $\sigma_{zz}=3.75\cdot\sigma_0$, while the maximum stress value σ_{yy} acting in the direction $\varphi=0$ is equal to $\sigma_{yy}=2.50\cdot\sigma_0$, and the maximum value of the stresses acting in the thickness direction is equal to $\sigma_{xx}=3.00\cdot\sigma_0$.

In the case of C(T) specimen with the relative crack length $a/W=0.20$, the maximum values of the successive normal components of the stress tensor is $\sigma_{zz}=3.90\cdot\sigma_0$, $\sigma_{yy}=2.50\cdot\sigma_0$ and $\sigma_{xx}=3.15\cdot\sigma_0$, whereas for a specimen with a relative crack length $a/W = 0.70$, the maximum values are at the level of $\sigma_{zz}=3.80\cdot\sigma_0$, $\sigma_{yy}=2.45\cdot\sigma_0$ and $\sigma_{xx}=3.0\sigma_0$. It can therefore be said that for a given material specification, the maximum value of successive normal components of the stress tensor is very slightly sensitive to the change in crack length. This confirms the conclusions given in the previous paper [25, 26]. The analysis of Fig.6 also proves the fact that the maximum value of the average stresses σ_m, is generally equal to the maximum stress value in the thickness direction, denoted by σ_{xx} and is equal to $3.00\cdot\sigma_0$, $3.15\cdot\sigma_0$ and $3.10\cdot\sigma_0$ for specimens characterized by relative crack length a/W equal to *0.05*, *0.20* and *0.70*, respectively.

Consideration of the distribution of normal components of the stress tensor presented in Fig.6 as a function of the normalized distance from the crack tip denoted by ψ is required to determine the maximum stress values opening the crack surfaces σ_{zz} and their normalized position relative to the crack tip, which is required to estimating the real fracture toughness using the selected fracture criteria – e.g. papers [18,25,26]. As it can be seen, the increase in external load is accompanied by a slight reduction in the normalized distance of the maximum stresses opening the crack surfaces to the crack tip – for the considered material characteristics, this value is around $\psi=1.00$. This is, therefore, twice a smaller distance than what O'Dowd and Shih [13, 14] have suggested as a place for measuring the Q stresses. The normalized distance of the maximum mean stresses from the crack tip for the considered geometry and material configuration is also $\psi=1.00$.

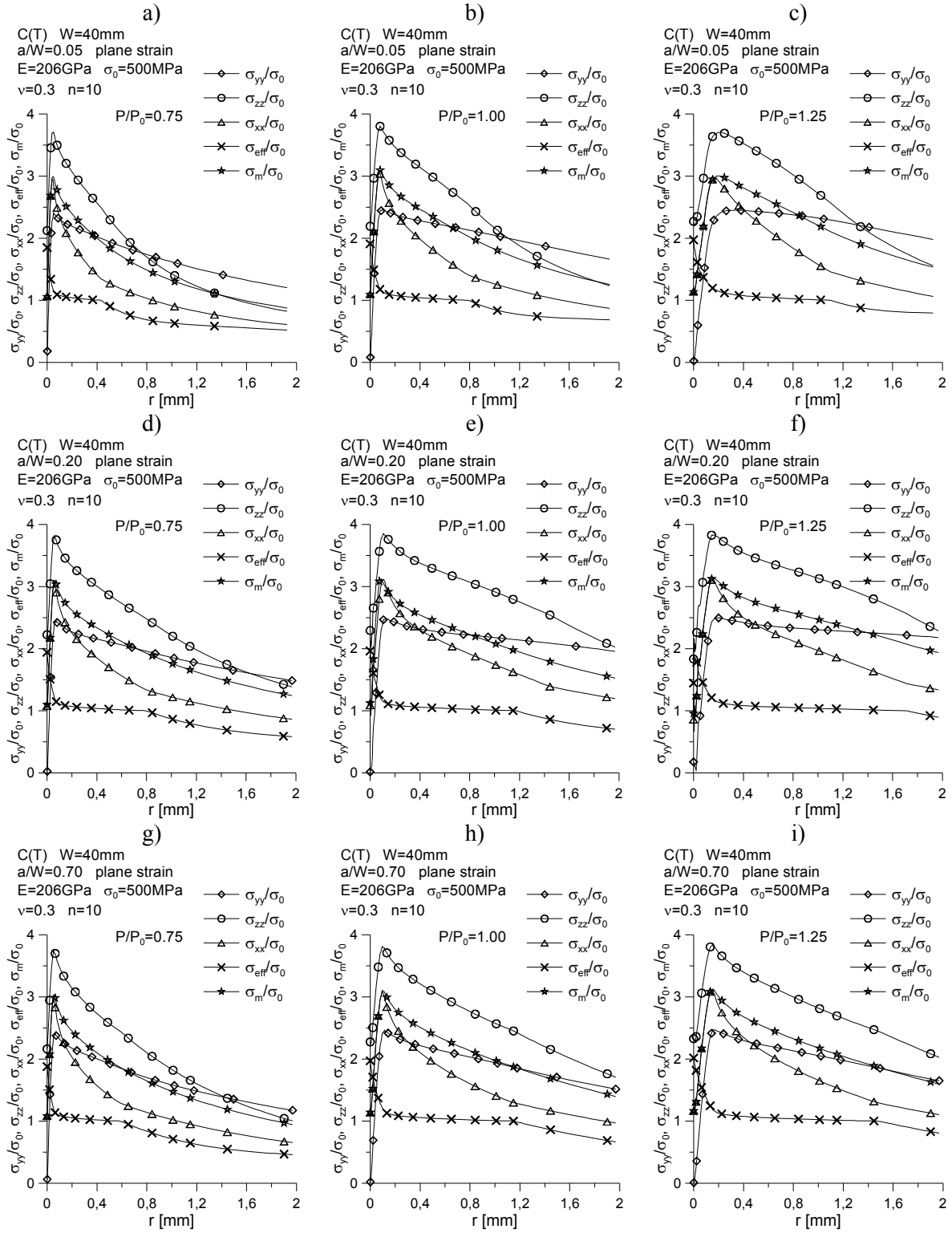

Fig.5. The stress distribution near the crack tip for C(T) specimen dominated by plane strain, estimated for direction φ=*0*, for the selected physical distance from the crack tip (denoted as *r*) and three levels of external load $P/P_0=\{0.75, 1.00, 1.50\}$: a,b,c) for C(T) with $a/W=0.05$; d,e,f) for C(T) with $a/W=0.20$; g,h,i) for C(T) with $a/W=0.70$.

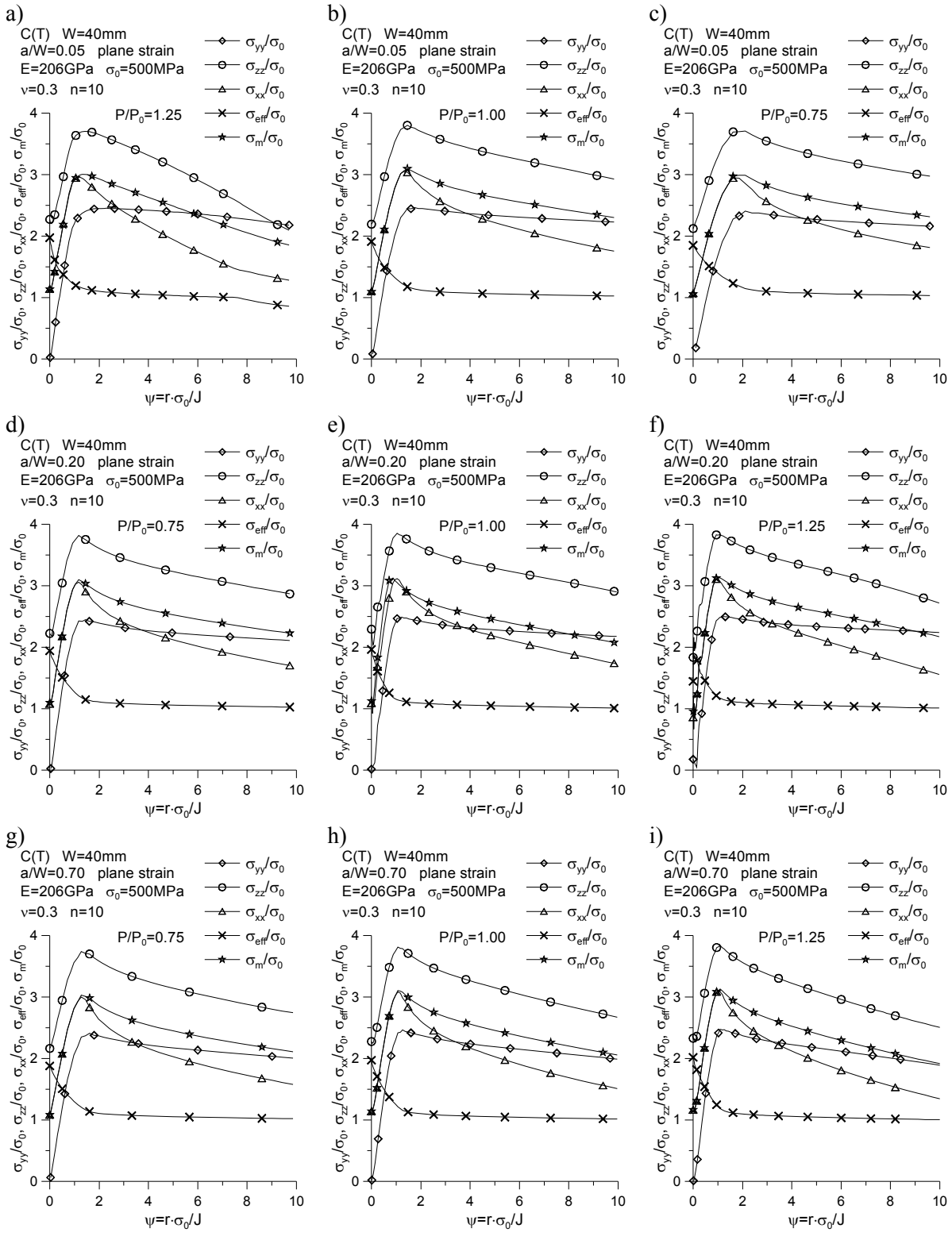

Fig.6. The stress distribution near the crack tip for C(T) specimen dominated by plane strain, estimated for direction $\varphi=0$, for the selected normalized distance from the crack tip (denoted as $\psi=r\cdot\sigma_0/J$) and three levels of external load $P/P_0=\{0.75, 1.00, 1.50\}$: a,b,c) for C(T) with $a/W=0.05$; d,e,f) for C(T) with $a/W=0.20$; g,h,i) for C(T) with $a/W=0.70$.

4.2. Analysis of the selected stress triaxiality parameters

Figures 7 and 8 present the distributions of the estimated principal stresses –denoted as σ_I, σ_{II} and σ_{III}, together with the set of changes of effective stresses and mean stresses, respectively in the function of the physical distance from the crack tip and the normalized distance, denoted by ψ. In many scientific papers, the main stresses are mentioned, and they are used to estimate various parameters of stress triaxiality, however, their distributions are rare or not discussed at all.

As we can see, the maximum of the principal stresses σ_I for the considered geometry should be identified with σ_{zz} stresses opening the crack surfaces. Minimum principal stresses, denoted by σ_{III}, in close proximity to the crack tip ($\psi=0\div1$) should be identified with the σ_{yy} stresses determined for the direction $\varphi=0$, after which their value is equal to the σ_{xx} stresses, which are measured in the direction of specimen thickness.

The analysis of Fig.8 shows that in the close vicinity of the crack tip (in the range of normalized distance $\psi=(0\div6)$), the distribution of principal stresses for the considered range of external loads takes the form described above. As mentioned above, the maximum level of mean stress σ_m, practically isn't sensitive to a change in the external load, as well as to a very small extent depending on the relative crack length. This value is usually three times the yield point (or *10÷15*% more). Some researchers used mean stresses to evaluate the real fracture toughness using the proper fracture criterion [40], and also this quantity was suggested by O'Dowd [13, 14] as the basis to estimate the Q stress, as a substitute for the crack opening stress – due to the inclusion of the mean stresses, the fact of triaxiality of stresses in structural elements dominated by a plane strain, or characterized by triaxility of strains and stresses is taken into account.

Figures 9 and 10 present numerically determined changes in the maximum principal stresses σ_I/σ_0 for the direction $\varphi=0$ (as said above, the distribution in the considered range of normalized distances is identified with the distribution of stress opening the fracture surfaces), the triaxiality parameter of stress σ_m/σ_{eff} (indicated by some as η– see formula (2.5)), effective stresses (their distribution sometimes allows to properly interpret the size of the plastic zone), the accumulation of plastic deformations ε_{aps} and the LODE parameter, estimated according to formula (2.8). The maximum value of the triaxiality of stress σ_m/σ_{eff} depends very little on the level of the external load and is practically insensitive to the crack length – its approximation is equal to $\sigma_m/\sigma_{eff}=2.65$ (Figs 9 and 10).

The physical position of this maximum in relation to the crack tip, together with the increase in the external load, increases, for the three considered levels of external load, the maximum is the case of C(T) specimen characterized by the shortest crack (Fig.9). On the other hand, considering the position of the maximum of the triaxiality of stresses in relation to the crack tip in normalized coordinates (Fig.10), it should be noted that with the increase of the external load, the value of the normalized position of the maximum parameter σ_m/σ_{eff} decreases, striving to reach a value set at around $\psi=1.75$ for specimens containing very short cracks (*a/W 0.05*) and $\psi=1.25$ for the remaining cases (*a/W=0.20* and *a/W=0.70*).

The external load has a very significant effect on the distribution of the LODE parameter near the crack tip (Figs 9 and 10). As we know, the LODE parameter value changes in the range LODE=$\langle -1; 1\rangle$ [32, 33]. The MES analysis carried out proves this (Fig.9) and shows changes along with the increasing external load. Starting from the crack tip, the value of the LODE parameter in its close vicinity oscillates around a value equal to zero, after which it drops to the value -1, then almost linearly increases to the value equal to 1, after which it drops again. In the range of the physical distance from the crack tip $r=\langle 0; 2\rangle mm$ considered in Fig.9, the graph presenting the changes of the LODE parameter is characterized by two extremes. As we can see, the location of these extremes changes – they move physically away from the crack tip, as the external load increases (Fig.9).

It can therefore be unequivocally stated that the changes of the LODE parameter as a function of the physical distance from the crack tip, strongly depends on the external load. A comparison of the following combinations from Fig.9, for the same external load and different relative crack lengths, indicates that the distribution of the LODE parameter as a function of the physical distance from the crack tip is also strongly dependent on the relative crack length. The greater the level of external load, the further extreme of the LODE parameter changes relative to the physical position relative to the crack tip (i.e., the extreme of the LODE parameter lie further from the crack tip).

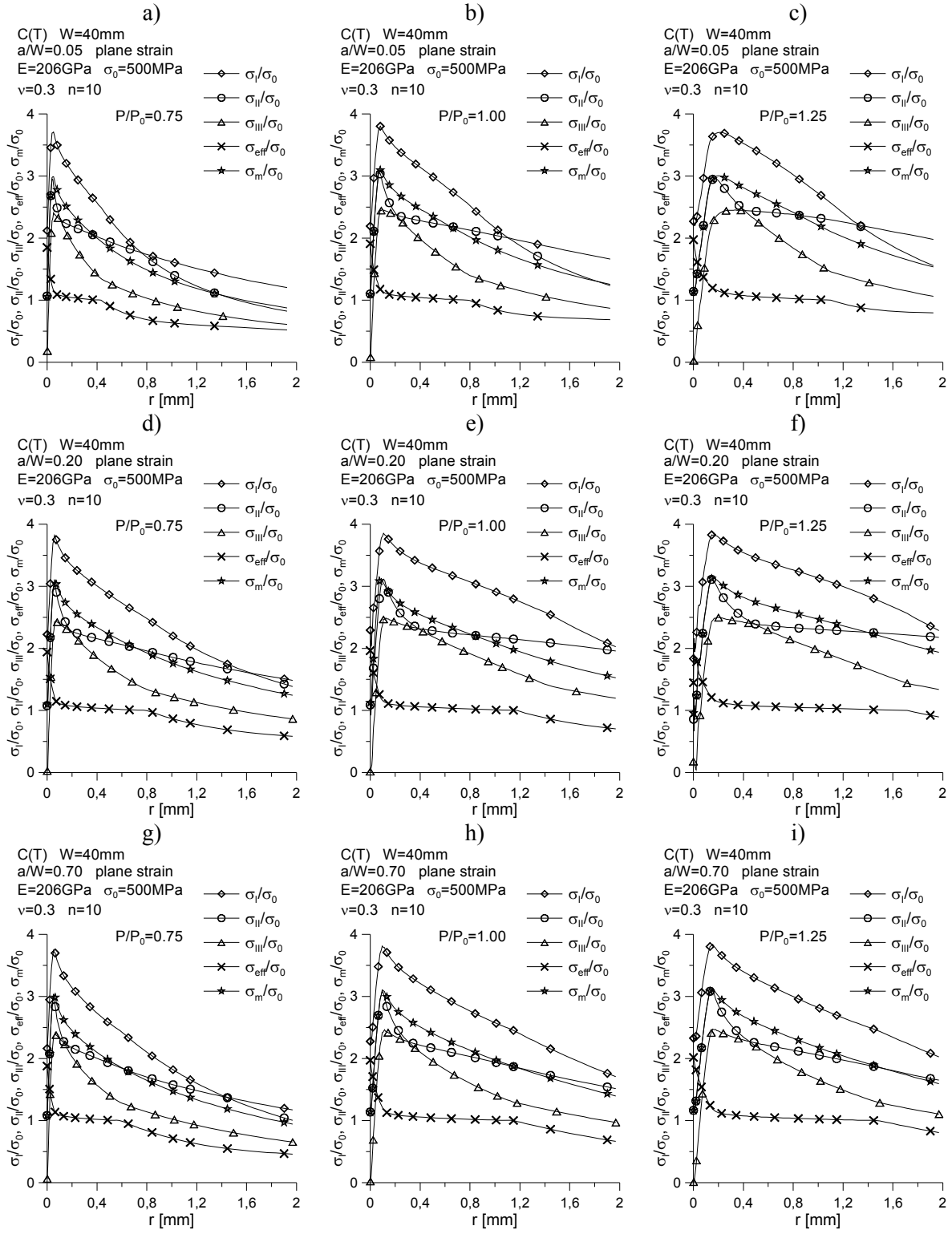

Fig.7. The principal stress distribution near the crack tip for C(T) specimen dominated by plane strain, estimated for direction $\varphi=0$, for the selected physical distance from the crack tip (denoted as r) and three levels of external load $P/P_0=\{0.75, 1.00, 1.50\}$: a,b,c) for C(T) with $a/W=0.05$; d,e,f) for C(T) with $a/W=0.20$; g,h,i) for C(T) with $a/W=0.70$.

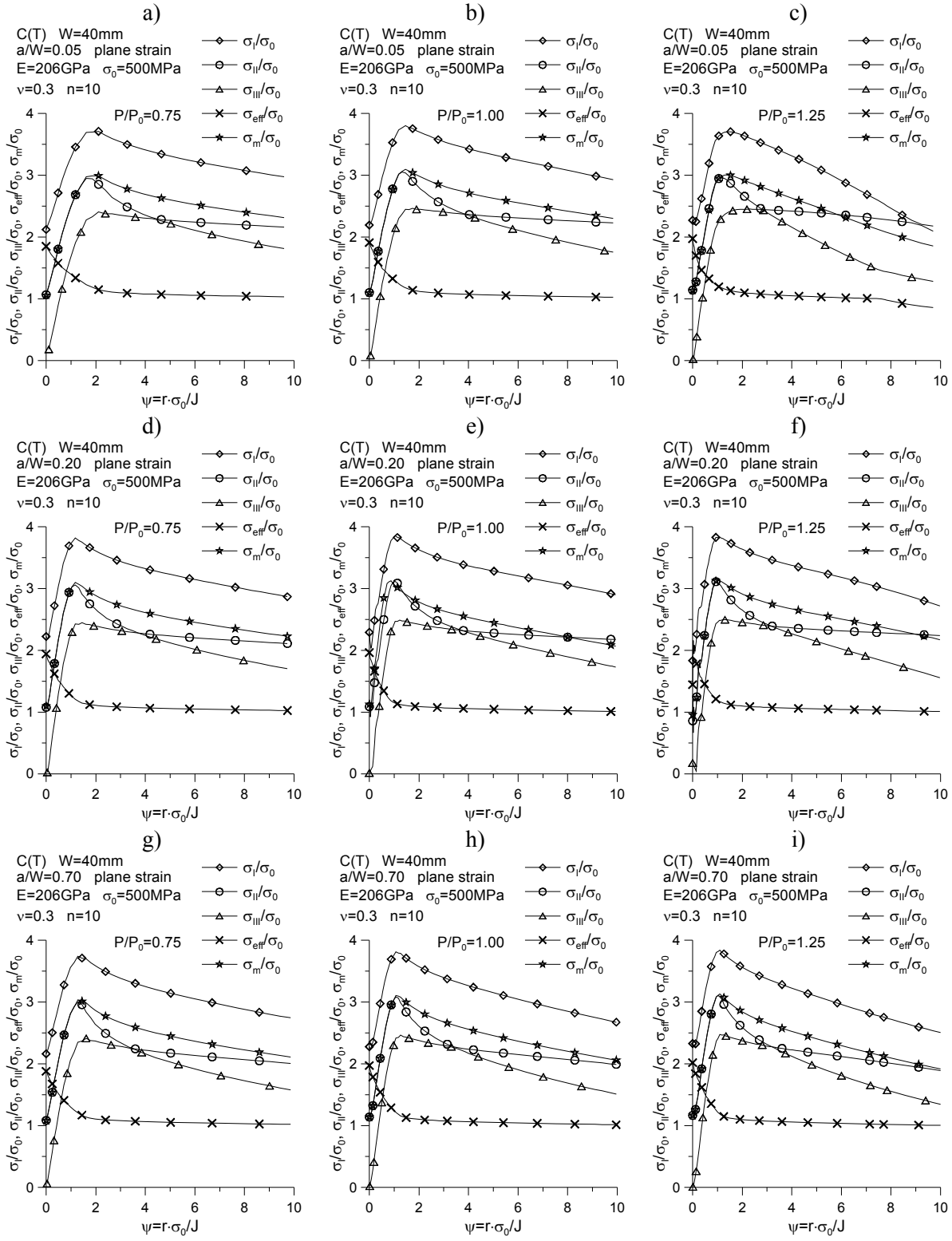

Fig.8. The principal stress distribution near the crack tip for C(T) specimen dominated by plane strain, estimated for direction φ=0, for the selected normalized distance from the crack tip (denoted as $\psi=r\cdot\sigma_0/J$) and three levels of external load $P/P_0=\{0.75, 1.00, 1.50\}$: a,b,c) for C(T) with $a/W=0.05$; d,e,f) for C(T) with $a/W=0.20$; g,h,i) for C(T) with $a/W=0.70$.

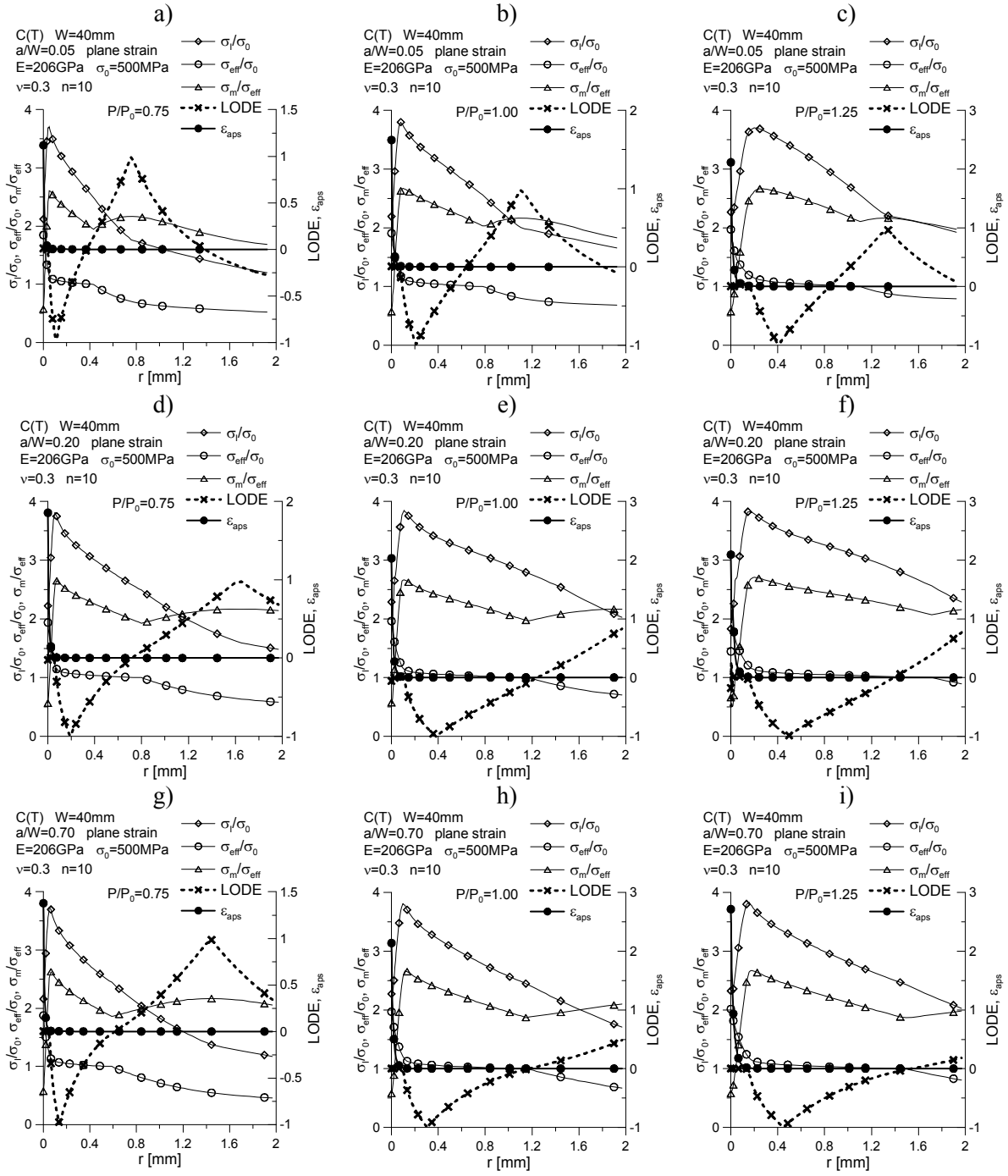

Fig.9. The comparison of the maximum principal stress (σ_I/σ_0), the effective stress (σ_{eff}/σ_0), the triaxiality parameter (σ_m/σ_{eff}), the LODE parameter and the accumulated plastic strains distributions near the crack tip for C(T) specimen dominated by plane strain, estimated for direction $\varphi=0$, f or the selected physical distance from the crack tip (denoted as r)and three levels of external load $P/P_0=\{0.75, 1.00, 1.50\}$: a,b,c) for C(T) with $a/W=0.05$; d,e,f) for C(T) with a/W=0.20; g,h,i) for C(T) with $a/W=0.70$.

The assessment of changes in the distribution of the LODE parameter as a function of the normalized position relative to the crack tip, denoted by ψ (Fig.10), leads to the following conclusions. With the increase of the external load, the minimum of the LODE parameter moves closer to the crack tip and for external load

$P/P_0=1.25$ it is at the level of $\psi=3$. The influence of the relative crack length on the normalized position ψ of this minimum is observable for external loads $P/P_0<1.00$.

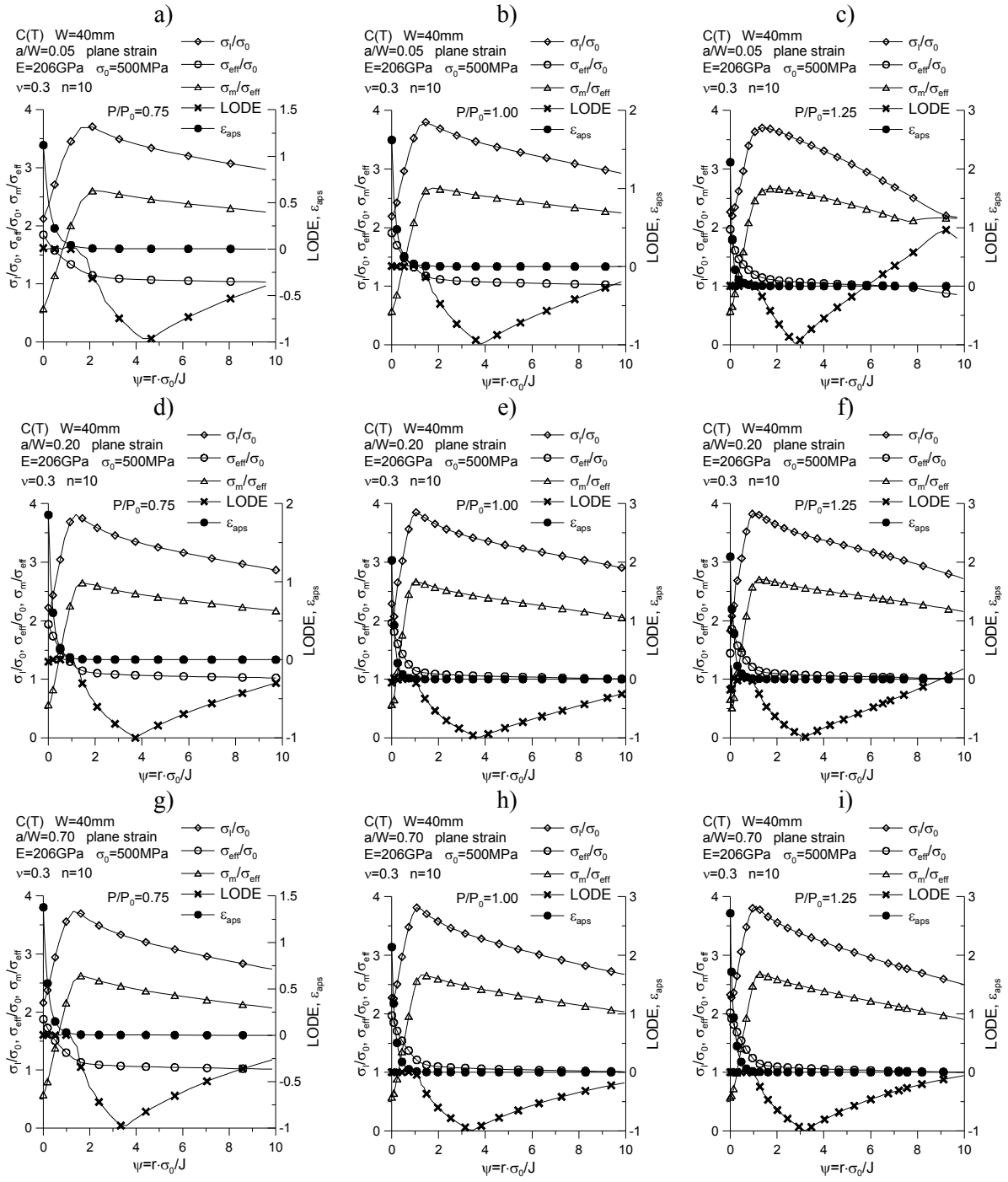

Fig.10. The comparison of the maximum principal stress (σ_I/σ_0), the effective stress (σ_{eff}/σ_0), the triaxiality parameter (σ_m/σ_{eff}), the LODE parameter (*LODE*) and the accumulated plastic strains (ε_{aps}) distributions near the crack tip for C(T) specimen dominated by plane strain, estimated for direction $\varphi=0$, for the selected normalized distance from the crack tip (denoted as $\psi=r\cdot\sigma_0/J$) and three levels of external load $P/P_0=\{0.75, 1.00, 1.50\}$: a,b,c) for C(T) with $a/W=0.05$; d,e,f) for C(T) with $a/W=0.20$; g,h,i) for C(T) with $a/W=0.70$.

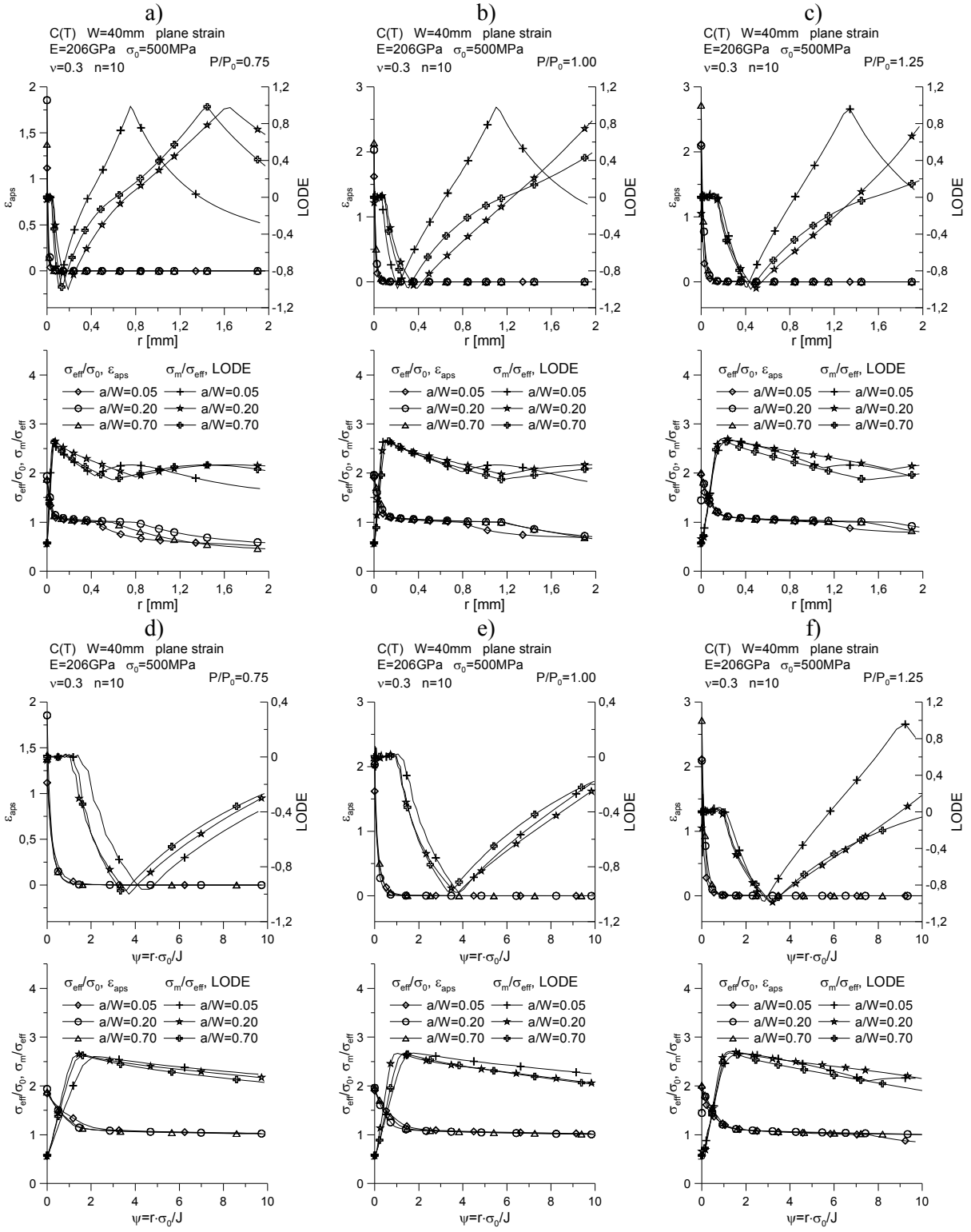

Fig.11. The comparison of the selected parameters of the stress and strain fields (ε_{aps}, LODE, σ_{eff}/σ_0, σ_m/σ_{eff}) near the crack tip for C(T) specimen characterized by a different relative crack length and three different levels of the external load P/P_0: a,b,c) graphs relative to the physical position r; d,e,f) graphs relative to normalized distance from the crack tip $\psi=r\cdot\sigma_0/J$.

Figure 11 presents a comparison of four parameters characterizing stress and strain fields near the crack tip (normalized effective stresses σ_{eff}/σ_0, stress bias parameter σ_m/σ_{eff}, LODE parameter and accumulated plastic strain ε_{aps}) for C(T) specimens with a different relative crack length, for three external load levels considered in this paper. The diagrams were drawn both in relation to the physical distance from the crack tip denoted by r, as well as in relation to the normalized distance from the crack tip denoted as ψ, calculated according to the expression $\psi=r\cdot\sigma_0/J$.

As it can be seen, the relative crack length practically does not affect the level of accumulated plastic strain ε_{aps}, normalized effective stresses, and the triaxiality parameter of stresses denoted as σ_m/σ_{eff}. This phenomenon is observed regardless of the level of considered external load. However, the significant effect of the relative crack length on the level and nature of changes the LODE parameter is visible – depending on the level of external load, the extremes of the LODE parameter are shifted and the value of which changes within the range $\langle -1,1\rangle$.

A similar comparison is presented in Fig.12, where, next to the normalized mean stresses σ_m/σ_0 and maximum principal stresses σ_I/σ_0, the changes in the Tz parameter defined by Guo Wanlin [37] are presented (this is the ratio of the stress measured in the direction of thickness σ_{xx} and sums of normal stresses opening the crack surfaces σ_{zz} and stresses operating in the direction $\varphi=0$ denoted as σ_{yy}, $Tz=\sigma_{xx}/(\sigma_{zz}+\sigma_{yy})$. When assessing the change of the above mentioned values in relation to the physical distance from the crack tip, one can notice a significant effect of the relative crack length on the distribution of mean and maximum principal stresses – for the shortest cracks ($a/W=0.05$), distributions $\sigma_m/\sigma_0=f(r)$ and $\sigma_I/\sigma_0=f(r)$ are the lowest. Curves representing changes in the Tz – $Tz=f(r)$ parameter behave similarly.

An analysis of the same distributions relative to the normalized distance from the crack tip denoted by ψ indicates a slight effect of the relative crack length on these values – differences for extreme curves change by about $10\div25$%, depending on the choice of the point near the crack tip. It can be noted that the value of the Tz parameter in close proximity to the crack tip, up to the location of the maximum of the stress opening the fracture surfaces, oscillates around the value of 0.5, characteristic for the domination of the plane strain state, which was marked in [37]. As we move away from the crack tip, the value of the Tz parameter decreases, striving for a value equal to the Poisson ratio assumed in the this paper and analysis as 0.3. The speed of these changes depends on the level of external load – the higher the external load, the further from the crack tip, the Tz parameter reaches a value equal to Poisson's ratio.

Figure 13 in the form of isoline diagrams shows the distribution of effective stresses (Figs 13a-c) and accumulated plastic strains (Figs 13d-f) for three C(T) specimens differing in the relative crack length $a/W=\{0.05,0.20,0.70\}$ at the moment when the external load reaches the value equal to the limit load. The yield strength assumed in the numerical calculations was $\sigma_0=500$MPa and it can be identified with the green color on the insulations shown in Figs 13a-c. The distribution of effective stresses, referred to the yield point, allows a visual assessment of the size of the plastic zone when the external load is equal to the limit load.

It can be noticed that only in the case of a specimen with a very long crack ($a/W=0.70$ - Fig.13c) the plastic zone in front of the crack tip covers all the uncracked ligament of the specimen – for this crack length the most visually largest crack opening displacement is observed (Fig.13f, drawings 13d-f were made on the same scale). In the case of C(T) specimens containing very short and short cracks ($a/W=0.05$ and $a/W=0.20$ respectively), an increase of the plastic zone around the crack tip is observed, and then further in the direction and place of the external load application (Fig.13a and Fig.13b). For these two geometries, there is no coverage of the entire uncracked section of the specimen through the plastic zone. In both cases – very short and short cracks, there is a significant crack opening displacement (Fig.13d and Fig.13e), however the highest level of accumulated plastic strains at the crack tip is observed for a specimens containing a very long crack ($a/W=0.70$) – Fig.13f. In this paper, the assessment of the crack opening displacement is carried out in a qualitative manner. Quantitative analysis, combined with a qualitative description will be presented soon in the next paper.

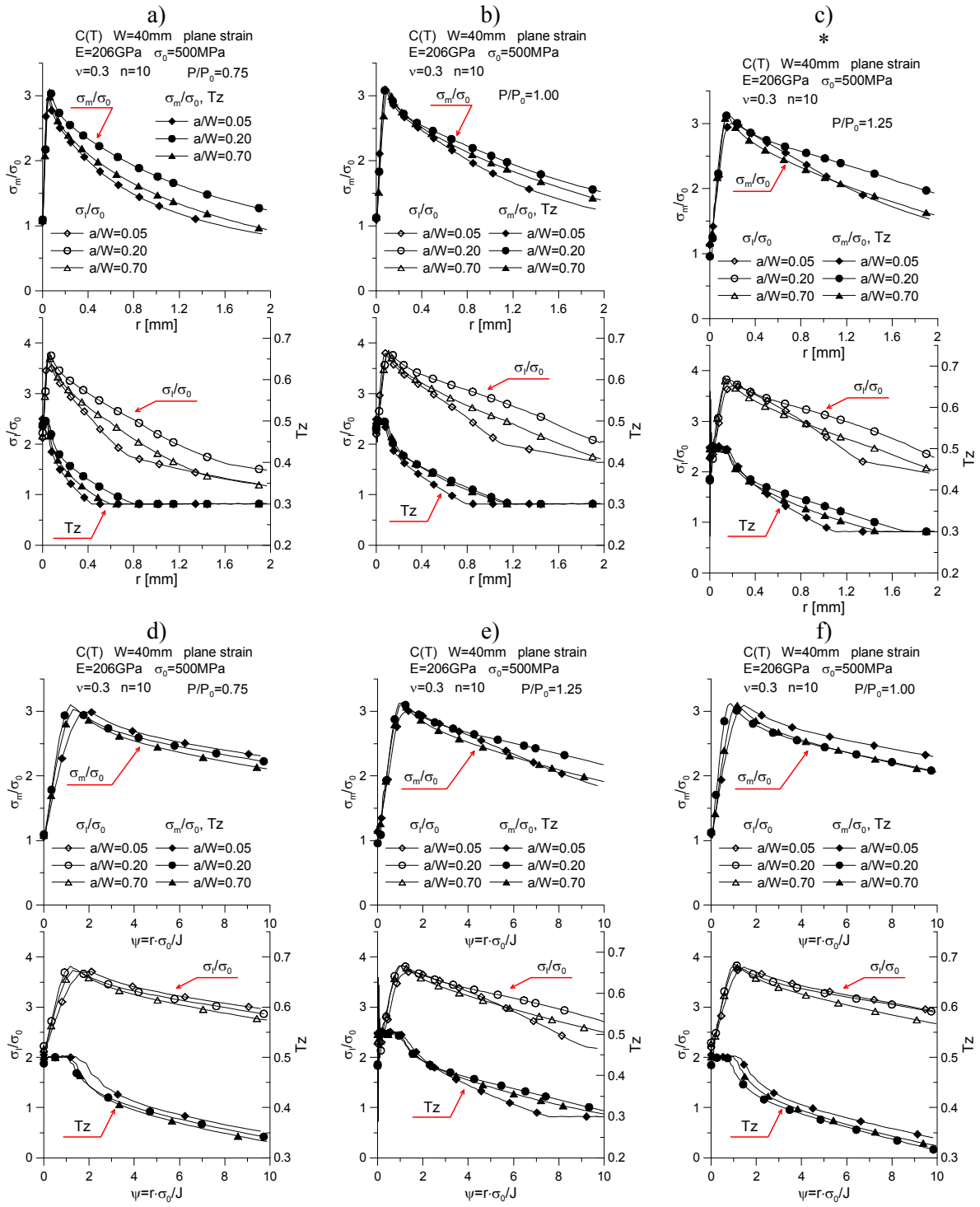

Fig.12. The comparison of the selected parameters of the stress fields (σ_l/σ_0, σ_m/σ_0, Tz) near the crack tip for C(T) specimen characterized by a different relative crack length and three different levels of the external load P/P_0: a,b,c) graphs relative to the physical position r; d,e,f) graphs relative to normalized distance from the crack tip $\psi=r\cdot\sigma_0/J$.

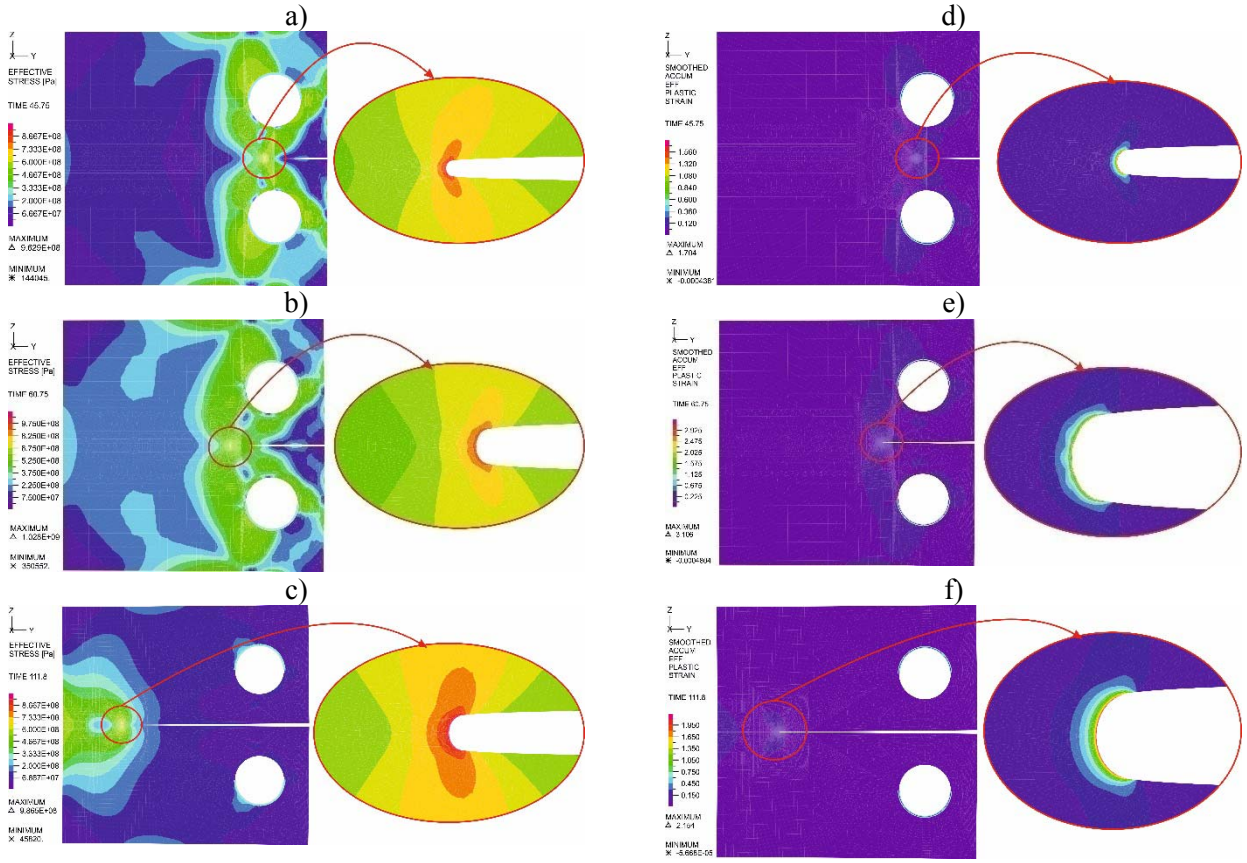

Fig.13 The distribution of the effective stress σ_{eff} and accumulated plastic strains for C(T) specimens dominated by plane strain (calculations for large strain assumptions) for material characterized by $n=10$, $\sigma_0=500$MPa, $E=206$GPa, $\nu=0.3$: a,b,c) the σ_{eff} stresses distribution for C(T) specimen characterized by $a/W=\{0.05, 0.20, 0.70\}$ respectively; d,e,f) ε aps strains distribution for C(T) specimen characterized by $a/W=\{0.05, 0.20, 0.70\}$ respectively (all results for external load $P/P_0=1.00$).

5. Summary

The paper presents an abbreviated characterization of the selected measures of the stress triaxiality for a compact specimen dominated by a plane strain state. Apart from short theoretical deliberations devoted to the description of stress fields near the crack tip, based on the results presented in [20,21], the basic measures of in-plane constraints used to assess the actual fracture toughness (Q stresses [13,14], maximum crack opening stresses[25, 26]), are discussed, as well as the formulas allowing to estimate the selected measures of stress triaxiality, which are discussed in [27, 30-33].

In the next step, the basics of FEM modeling were briefly characterized, based on the considerations given in [20,21]. In the considerations based on the numerical calculations, an elastic-plastic material was assumed, characterized by hardening exponent $n=10$ and the ratio of the yield point and Young's modulus $\sigma_0/E=0.00243$, with the Poisson coefficient $\nu=0.3$. Specimens characterized by three relative crack lengths were analyzed – among them one can distinguish very short, short and very long cracks ($a/W=\{0.05, 0.20, 0.70\}$ respectively). The numerical analysis was carried out with the assumption of finite deformations, which guarantees the elimination of singularities of stresses near the crack tip. A quality assessment (as well as in some places of the paper by quantitative assessment) of the selected parameters was performed on the distribution of normal components of stress tensor, distribution of effective stresses, distribution of mean

stresses as well as principal stresses (whose estimation is necessary for the analysis of selected parameters of stress triaxiality). Then, the selected values of stress triaxiality were subjected to the analysis and qualitative evaluation, among which the LODE parameter, triaxiality coefficient denoted as σ_m/σ_{eff}, the *Tz* parameter, as well as the accumulated plastic strains can be mentioned.

The performed analysis indicated some important conclusions. The highest value among the normal components of the stress tensor is reached by the stress opening the crack surfaces indicated by σ_{zz}. In view of the assumption of the finite strain in FEM analysis, the normal components of stress tensor at a certain distance from the crack tip reach the maximum – generally after exceeding the external load at *75*% of the limit load, the value of this maximum does not depend on the external load level, however with the increase of external load, this maximum physically moves away from the crack tip. When assessing the normalized location of the stress maximum denoted as$\psi=r\cdot\sigma_0/J$, it should be noted that if the external load increases above the limit load, it also does not depend on the external load.

The above-mentioned statements indicate the fact that in the considered external loads range, the level of maximum stresses opening the fracture surfaces and their normalized location relative to the crack tip do not depend on the relative crack length, which confirms the conclusions given in [25, 26]. As the numerical analysis has shown, the stresses that open the fracture surfaces should be identified with the maximum principal stresses. The selected measures of the triaxiality of stress discussed in the paper – LODE parameter, *Tz* parameter and the stress triaxiality parameter σ_m/σ_{eff} (determined by some researchers as η [27, 30, 32, 33]), depend on the level of external load, relative crack length and position in relation to the crack tip. The analysis of the isolines presenting the distribution of effective stresses allows to assess the position and size of the plastic zone. As numerical analysis showed, the full coverage of the uncracked ligament of the specimen for external load equal to the limit load was observed for C(T) specimens characterized by a very long crack (*a/W=0.70*), while for specimens containing very short and short cracks (respectively *a/W=0.05* and *a/W=0.20*), the plastic zone grows in close proximity to the crack tip and the areas identified with the places of application of the external load.

Summing up, conducting a comprehensive numerical analysis should include not only analysis of stress or strain tensor distributions, but also an assessment of geometric constraint parameters, stress triaxiality parameters, assessment of accumulated plastic deformations, and level of plastic zones. The analysis should be carried out in a quantitative and qualitative manner. In addition, the level of the J-integral or crack opening displacement can be assessed, and all the drawn conclusions can be used in the correct description of mechanical fields, predicting the real fracture toughness (using the appropriate fracture criterion) or assessing the strength of the structure containing some defect, using the FAD (Failure Assessment Diagrams) or CDF (Crack Driving Force) diagrams [34-36].

Acknowledgements

The research reported herein was supported by a grant from the Faculty of Mechatronics and Machine Design at Kielce University of Technology (project No. 01.0.09.00/2.01.01.01.0027 MNSP.MKTM.17.002).

Nomenclature

ASTM – American Society Testing Materials
A_2 – A_2 parameter, described also as A_2 amplitude defined by Yang *et al.*
a – crack length
a/W – relative crack length
B – specimen thickness
BS – British Standard
b – length of the uncracked ligament ($b=W-a$)
C(T) – compact specimen
CC(T) – center cracked plate in tension

E – Young's modulus
EPRI – Electric Power Research Institute
ESIS – European Structural Integrity Society
FAD – Failure Assessment Diagram
FE – Finite Element
FEM – Finite Element Method
FITNET – European FITness-for-service NETwork
HMH – Huber-Misses-Hencky hypothesis
HRR – Hutchinson-Rice-Rosengren
J – J-integral
J-R – J-R curves (graphical presentation of the change of the J-integral as a function of the crack growth length da)
L, LODE – Lode parameter
MCOS – Maximum Crack Opening Stress
n – strain hardening exponent in the Ramberg-Osgood relationship
P – external load
P_0 – limit load
Q – Q-stress parameter defined by O'Dowd and Shih, the measure of the in-plane constraints for elastic-plastic materials
RKR – Ritchie-Knott-Rice
R-O – Ramberg - Osgood
r – physical distance from the crack tip, polar coordinate
r_w – radius of the crack tip in the finite element model
SEN(B) – single edge notched cracked plate in bending
SEN(T) – single edge notched cracked plate in tension
Tz – stress triaxiality parameter defined by GuoWanlis as $\sigma_{xx}/(\sigma_{yy}+\sigma_{zz})$
v_{LL} – load line displacement
W – specimen width
x_{22_max} –physical location of the maximum stress opening the crack surfaces
x, y, z – Cartesian coordinates – x is the coordinate in the direction of the specimen thickness
α – constant in the Ramberg-Osgood relationship
ε – strain on stress-strain curve
ε_0 – strain corresponding to the yield stress ($\varepsilon_0=\sigma_0/E$)
ε_{aps} – accumulated plastic strain
ε_m – strain corresponding to the ultimate tensile strength
ν – Poisson's ratio
φ – polar coordinate
θ – Lode angel
$\bar{\theta}$ –normalized Lode angel
$[\sigma]$ – stress tensor
[S] –deviatoricstress tensor
[I] –identity tensor
η –dimensionless hydrostatic stress triaxiality parameter
η_0 –reference value of the triaxiality parameter dented as η
σ –stress on stress-strain curve
$\sigma_1, \sigma_2, \sigma_3$ –principal stresses, also denoted as $\sigma_{\mathrm{I}}, \sigma_{\mathrm{II}}, \sigma_{\mathrm{III}}$
σ_0 – yield stress
σ_{eff} – effective stresses calculated according to the HMH hypothesis
σ_{ij} – stress tensor
σ_{22_FEM} – crack opening stress determined using FEM
σ_{22_HRR} – crack opening stress determined using HRR solution
σ_{22_max} – maximum of the crack opening stress
σ_m – normal stresses
σ_{yld} – yield stress defined by Wierzbicki and Bai

σ_{xx}, σ_{yy}, σ_{zz} – normal components of the stress tensor
$\bar{\sigma}\left(\overline{\varepsilon_p}\right)$ – relation between effective real stress and accumulated plastic strain
ψ – normalized distance from the crack tip, calculated as $\psi = r \cdot J/\sigma_0$
ψ_0 – normalized positon near the crack tip of the MCOS for saturate state
ξ_0 – normalized maximum opening crack stress for saturate state

References

[1] ASTM (2005): ASTM E 1820-05 *Standard Test Method for Measurement of Fracture Toughness*. − American Society for Testing and Materials.

[2] ASTM (2011): ASTM E1921-11 *Standard test method for determining of reference temperature T0 for ferritic steels in the transition range*. − American Society for Testing and Materials.

[3] BS 5762. *Methods for crack opening displacement (COD) testing*. − London: British Standards Institute; 1979.

[4] BS 7448: *Part 1. Fracture mechanics toughness tests: Part 1 – Method for determining of K_{Ic}, critical CTOD and critical J values of metallic materials*. − London: British Standards Institute; 1991.

[5] PN-87/H-4335, *Metals – Test method for measurement of the fracture toughness for plane strain conditions*.

[6] Kornev V.M. and Demeshkin A.G. (2018):*Quasi-brittle fracture of compact specimens with sharp notches and U-shaped cuts*.− Journal of Applied Mechanics and Technical Physics, vol.59, No.1, pp.120-131, DOI 10.1134/S0021894418010157.

[7] Kayamori Y. and Kawabata T. (2017):*Evaluation of rotational deformation in compact specimens for CTOD fracture toughness testing*. − DOI 10.1016/j.prostr.2017.07.135.

[8] Doddamani S. and Kaleemulla M. (2017):*Fracture toughness investigations of Al6061-graphite particulate composite using compact specimens*.− FratturaedIntegritàStrutturale,vol.11, No.41, pp.484-490, DOI 10.3221/IGF-ESIS.41.60.

[9] Horstman R.T., Lieb K.C., Power B., Landes J.D., et al (1979):*Evaluation of the J Integral for the Compact Specimen*. − Journal of Testing and Evaluation, vol.7, No.5, DOI 10.1520/JTE10222J.

[10] Shivakumar N. and Newman J.C. (1992):*Verification of effective thicknesses for side-grooved compact specimens*.− Engineering Fracture Mechanics, vol.43, No.2, DOI 10.1016/0013-7944(92)90125-X, Source NTRS,

[11] HuJ.M., Cheng J., Albrecht P. and Joyce J. (1989):*Ductile Crack Extension in Compact Specimens at Limit Load*.− DOI 10.1016/B978-0-08-034341-9.50047-4, In book: Proceedings of The 7th International Conference On Fracture (ICF7)

[12] Zhu X.-K. and Joyce J.A. (2012): *Review of fracture toughness (G, K, J, CTOD, CTOA) testing and standardization*. − Engineering Fracture Mechanics, vol.85,pp.1–46, doi:10.1016/j.engfracmech.2012.02.001.

[13] O'Dowd N.P. and Shih C.F. (1991): *Family of crack-tip fields characterized by a triaxiality parameter – I. Structure of Fields*. − J. Mech. Phys. Solids, vol.39, No.8, pp.989-1015.

[14] O'Dowd N.P. and Shih C.F. (1992): *Family of crack-tip fields characterized by a triaxiality parameter – II. Fracture Applications*. − J. Mech. Phys. Solids, vol.40, No.5, pp.939-963.

[15] Yang S., Chao Y.J. and Sutton M.A. (1993): *Higher order asymptotic crack tip fields in a power-law hardening material*. − Engineering Fracture Mechanics, vol.19, No.1, pp.1-20.

[16] Hutchinson J.W. (1968): *Singular behaviour at the end of a tensile crack in a hardening material*. − Journal of the Mechanics and Physics of Solids, vol.16, No.1, pp.13-31.

[17] Rice J.R. and Rosengren G.F. (1968): *Plane strain deformation near a crack tip in a power-law hardening material*. − Journal of the Mechanics and Physics of Solids, vol.16, No.1, pp.1-12.

[18] Neimitz A., Graba M. and Gałkiewicz J. (2007): *An alternative formulation of the Ritchie-Knott-Rice local fracture criterion*. − Engineering Fracture Mechanics, vol.74, pp.1308-1322.

[19] Ritchie R.O., Knott J.F. and Rice J.R. (1973): *On the relationship between critical tensile stress and fracture toughness in mild steel*. − Journal of the Mechanics and Physics of Solids,vol.21, pp.395-410.

[20] Graba M. (2018): *Characterization of the stress fields near crack tip for compact specimen for elastic-plastic materials in plane strain state domination*. − Book of abstracts of 41st Solid Mechanics Conference – SOLMECH 2018, paper number P262, pp.524-525.

[21] Graba M. (2019): *Characterization of the stress fields near crack tip for C(T) specimen for elastic-plastic materials for plane strain*. − International Journal of Applied Mechanics and Engineering, vol.24, No.3, pp.549-576.

[22] Graba M. (2011): *The influence of material properties and crack length on the Q-stress value near the crack tip for elastic-plastic materials for single edge notch plate in tension*. − Archives of Civil and Mechanical Engineering, vol.11, No.2, pp.301-319

[23] Graba M. (2012): *The influence of material properties and crack length on the Q-stress value near the crack tip for elastic-plastic materials for centrally cracked plate in tension*. − J. Theor. Appl. Mech., vol.50, No.1, pp.23-46.

[24] Graba M. (2008): *The influence of material properties on the Q-stress value near the crack tip for elastic-plastic materials*. − Journal of Theoretical and Applied Mechanics, vol.46, No.2, pp.269-290.

[25] Graba M. (2012): *Catalogue of the numerical solutions for SEN(B) specimen assuming the large strain formulation and plane strain condition*. − Archives of Civil and Mechanical Engineering, Published by Elsevier, vol.12, No.1, pp.29-40.

[26] Graba M. (2017): *A numerical analysis of selected elastic-plastic fracture parameters for DEN(T) plates under plane strain conditions*. − International Journal of Applied Mechanics and Engineering, vol.22, No.1, pp.49-80, DOI: https://doi.org/10.1515/ijame-2017-0004.

[27] Bai Y., Teng X. and Wierzbicki T. (2009): *On the application of stress triaxiality formula for plane strain fracture testing*. − J. Eng. Mater. Technol., vol.131, No.2, 021002, DOI: 10.1115/1.3078390.

[28] McClintock F.A.(1968): *A criterion of ductile fracture by the growth of holes*. − ASME J. Appl. Mech., vol.35, pp.363-371.

[29] Rice J.R. and Tracey D.M. (1969): *On the ductile enlargement of voids intriaxial stress fields*. − J. Mech. Phys. Solids, vol.17, pp.201-217.

[30] Bai Y. and Wierzbicki T. (2008): *A new model plasticity and fracturewith pressure and Lode dependence*. − Int. J. Plast., vol.24, pp.1071-1096.

[31] Neimitz A., Galkiewicz J. and Dzioba I.R. (2018): *Calibration of constitutive equations under conditions of large strains and stress triaxiality*. − Archives of Civil and Mechanical Engineering, vol.18, No.4, pp.1123-1135, DOI: 10.1016/j.acme.2018.02.013.

[32] Bao Y. and Wierzbicki T. (2004): *On fracture locus in the equivalent strain and stress triaxiality space.*− International Journal of Mechanical Science, vol.46, pp.81-98.

[33] Bai Y. and Wierzbicki T. (2010): *Application of extended Mohr–Coulomb criterion to ductile fracture.*− International Journal of Fracture, vol.161, pp.1-20.

[34] Kumar V., German M.D. and Shih C.F. (1981): *An engineering approach for elastic-plastic fracture analysis*. − Electric Power Research Institute, Inc. Palo Alto, CA, EPRI Report NP-1931.

[35] Graba M. (2013): *Extension of the concept of limit loads for 3D cases for a centrally cracked plate in tension*. − Journal of Theoretical and Applied Mechanics, vol.51, No.2, pp.349-362.

[36] Graba M. (2017): *Proposal of the hybrid solution to determining the selected fracture parameters for SEN(B) specimens dominated by plane strain*. − Bulletin of the Polish Academy of Sciences-Technical Sciences, vol.65, No.4, pp.523-532.

Received: April 11, 2019

Revised: June 24, 2019